THE PENNSYLVANIA STATE UNIVERSITY
SCHREYER HONORS COLLEGE

DEPARTMENT OF ENGINEERING SCIENCE AND MECHANICS

AN ACOUSTICALLY ENHANCED HOMOGENEOUS IMMUNOASSAY

NICOLAS MESYNGIER
SPRING 2017

A thesis
submitted in partial fulfillment
of the requirements
for a baccalaureate degree
in Engineering Science
with honors in Engineering Science

Reviewed and approved* by the following:

Tony Huang
Professor of Mechanical Engineering and Material Science
Thesis Supervisor

Barbara Shaw
Professor of Engineering Science and Mechanics
Honors Adviser

Judith A. Todd
Department Head
P.B. Breneman Chair and Professor
of Engineering Science and Mechanics

* Signatures are on file in the Millennium Scholars Program office.

ABSTRACT

Biomarker detection is an exciting field as new technologies are being developed for more sensitive and robust detection. Among existing techniques, there exists a need for a point-of-care, biocompatible, and affordable alternative to laboratory standards. In this work, the possibility of an acoustically enhanced homogeneous immunoassay is explored. To confirm the viability of our design, three steps were taken to validate our assay. First, enrichment of micro-/nanoparticles is demonstrated by actuating a single vortex flow within a glass capillary that combines the acoustic radiation force and the acoustic streaming force. Second, a simplified, two-part assay is tested for functionality and sensitivity. Having displayed a clear linear correlation between concentration and fluorescent intensity, a three-part assay is prepared and tested as well. The results from these studies are promising and provide a novel method for biomarker detection that could be used within a point-of-care platform in the future.

TABLE OF CONTENTS

LIST OF FIGURES

ACKNOWLEDGEMENTS

I would like to thank Prof. Tony Huang, my thesis advisor, for supporting this project and providing me guidance in discovering my passions. I would also like to thank Prof. Costanzo for serving as my co-advisor and helping me through the process of completing this thesis. I am very grateful for Prof. Peng Li and graduate student Zhangming Mao for serving as mentors within the lab and thoughtful discussions that helped shape this project. I would like to thank Prof. Shaw, my academic advisor, for helping enable me to pursue my passions. I would also like to thank Star Sharp, the program director of the Millennium Scholars Program, for her never-ending support and encouragement.

Separately, I would like to thank my family for all the support they have provided me with to allow me to pursue my passions and focus on my goals. Without them, none of this would have been possible.

This project was supported by the National Institute of Health (R01 HD086325) and the National Science Foundation (IDBR-1455658).

Introduction

When a patient walks into a doctor's office, four contributing factors are considered when attempting to make a diagnosis: the information provided by the patient, a patient's medical history, a physical examination and any diagnostic tests that can be used to provide further information.[1,2] The first two factors are used to ascertain a list of possible conditions as well as the likelihood of those possibilities based on a patient's personal and family medical history. The physical examination is the first step in collecting data about symptoms from the patient. Once all of this information is gathered, the doctor has a list of possible diagnoses. To confirm that any of the possible diagnoses are true, further tests must be used. The diagnostic tests chosen by the doctor are situationally dependent and can range from imaging, such as an x-ray or CAT scan, to a blood test.[3] One category of diagnostic tests are assays that measure the presence, and sometimes the concentration, of certain molecules that provide information about the condition of a patient. The specific molecules that are being measured are known as biomarkers. These molecules can provide a wide range of information from the level of inflammation in tissue to the functionality of an organ to the presence of an infection or cancer. Biomarkers can be any biological molecule that is known to correlate with a specific condition, including cells,[4] proteins,[5,6] peptides,[7] RNA,[8] exosomes,[9,10] or hormones.[11]

ELISA

Biomarker detection and quantification is necessary for diagnostic purposes, so methods are needed that provide the best balance of a number of factors based on the situation. Factors that should be considered when characterizing a biomarker test include precision, sensitivity, accuracy, resolution, specificity, cost, size, throughput, ease-of-use and turnaround time. A number of different tests exist depending on the needs of a given situation, but the most common test, and gold standard for laboratory detection is enzyme-linked immunosorbent assay (ELISA).

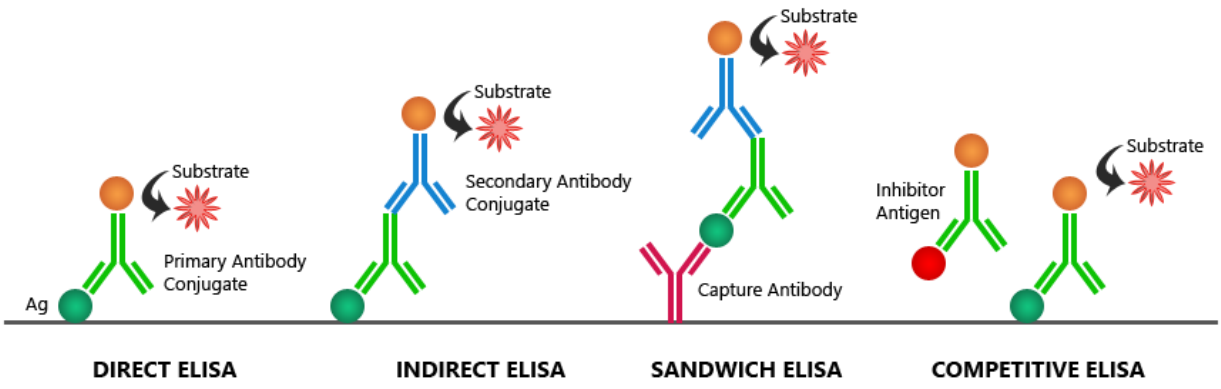

Figure 1: Sample ELISA configurations[12]

ELISA can be performed in a number of different configurations, but is generally conducted within a well plate and relies on a detection enzyme that emits an optical signal when it is able to properly connect to the target. ELISA configurations have two subsets, direct and indirect, and these can refer to both the immobilization of the target and the detection of the target. The first step in ELISA is the immobilization of the target. In direct immobilization, the solution being measured is placed within a well and all the molecules are allowed to non-specifically bond to the bottom of the plate. For indirect immobilization, antibodies specific to the target are first immobilized on the well. Then, the solution is placed in the well for a period of time to allow

interaction between the antibody and target. The well is then washed to remove any molecules that have not bonded to the immobilized antibodies. Once the target is immobilized on the bottom of the well, it needs to be detected.

In direct detection configurations, an antibody complimentary to the target is linked to a detection enzyme and added to the well where it can bond with the target of the assay. A washing step is used to eliminate any non-bonded antibodies and then a substrate is introduced to induce a detectable interaction with the detection enzyme. The intensity of the signal correlates with the concentration of the target. Indirect detection methods are similar, with an intermediate antibody added in the process. In this scenario, an (primary) antibody is added that bonds to the immobilized target. After a washing step, a secondary antibody is introduced that is attached to a detection enzyme. After another washing step, detection is conducted the same way as with direct detection. The advantage of indirect detection is that more than one secondary antibody can bond to the primary antibody, resulting in an enhanced signal. The advantages of direct detection are the elimination of an extra washing step, as well as any possible cross-reactivity with the secondary antibody. The detection enzyme can also be replaced with a different marker (fluorescent, Raman etc.) to create a very similar assay that is not technically an ELISA. ELISA tests are often used because of their high sensitivity, accuracy, specificity and throughput.

ELISA is used in situations where careful quantification is important and is therefore conducted in a laboratory setting. ELISA is common in research laboratories as well as in centralized medical facilities. These situations call for many samples to be tested at once for the same biomarker and therefore the plate-well structure is advantageous. In other situations, an easier to use and faster test is preferred that provides qualitative results. An example comparison would be detection of Cystatin-C, a kidney function biomarker where small shifts in

concentration are important,[13] vs a pregnancy test where the relevant information is whether or not the test subject is pregnant. In the second example, the person buying and using the test does not care about the specific amount of human chorionic gonadotropin in her system, just if enough is present to prove she is pregnant. In these type of scenarios, lateral flow assays (LFA) are common.

Lateral Flow Assays

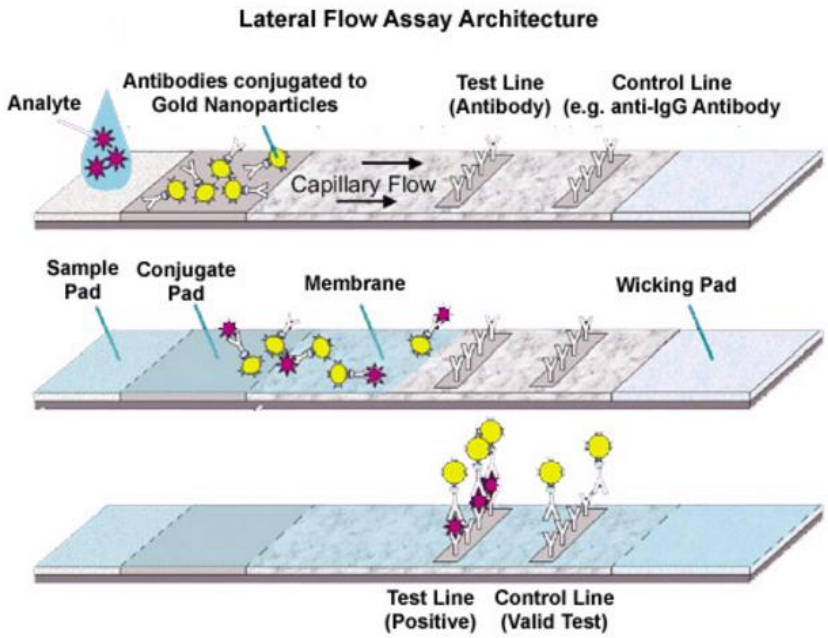

Figure 2: Schematic of a Sample Lateral Flow Assay. Top: Sample added to test strip, Middle: Analyte binds to conjugated nanoparticles Bottom: Test lines examined to read result of assay[14]

LFAs, or strip tests, are single-use tests that do not require any trained personnel to operate. LFA rely on capillary action to move a liquid sample across a series of regions that are functionalized to create specific interactions with a target analyte. The test is composed of six different components all connected on a substrate to improve the stability of the test. The sample

being tested is added to the “sample pad” at one end of the strip. This region contains surfactants and buffer salts to assist with future interactions further down the strip. The sample then travels along the strip towards the “conjugate pad” where micro-/nanoparticles functionalized with antibodies specific to the analyte are present. The particles are generally latex or colloidal gold and either fluorescent or colorful to allow for easy detection. The sample then travels further down the strip towards a detection zone, which contains both a test line and a control line. The detection zone is composed of a porous membrane to allow for the motion of the particles with or without attached biomarker targets. Within the detection zone is a test strip composed of a line of antibodies for the biomarker target. If the biomarker is present, it attaches to the test line, and the particles can be easily detected. Following the test line is a control line with antibodies to capture the particles that do not have an attached analyte. This strip is used as a check to ensure that the sample was able to properly flow along the strip. At the end of the strip opposite the sample pad is an absorbent pad that creates capillary motion. This moves the sample across the strip and also removes the remaining sample and particles that do not interact in the detection zone. The entire process takes 5-30 minutes and provides a qualitative result that can easily be read by simply looking at the location of the two lines. If two lines are present, the target biomarker is present; if there is only one line it is absent. LFAs are also homogeneous (wash-free), and therefore easier to use than ELISA.

Aggregation Assays

Another important category of biomarker assays are aggregation assays which are classified together because they all fundamentally depend on the aggregation of particles for detection. The

simplest example of an aggregation assay is the agglutination assay. In this assay, a target analyte is mixed into a solution containing micro-/nanoparticles that have been functionalized with a capture molecule (often an antibody) specific to the target. Initially, the solution is uniform, in turbidity and color. After gentle mixing, the functionalized particles begin bonding with the analyte (if it is present) and forming an aggregate. Note that for this test to work, the target must be able to bind with an antibody at multiple locations on the molecule. Once the particles begin aggregating together, a property of the solution changes which can be detected either visually or with the help of a specialized tools. Examples of agglutination assays include latex agglutination tests in which functionalized .9 μm latex particles are used as the capture mechanism.[15,16] If the target is present, the aggregates that form are sufficiently large that they can be visualized with the naked eye as small particles within the solution. If no target is present, the solution appears entirely uniform. Another variant of the agglutination assay uses gold or silver nanoparticles and their unique optical properties for detection.[17] The localized surface plasmon resonance of these metal nanoparticles results in strong absorption peaks that change based in size, shape and inter-particle distance. By using these particles in agglutination assays, a discernable color change can be detected when aggregation occurs, for example from red to blue, as the target analyte is added to the solution. Detection of DNA and RNA can be done using a similar configuration but with strands complementary to the start and end of the target added to particles. If the target DNA/RNA is present it serves as the linker between particles, bringing them close together.

Another assay that relies on the aggregation of particles is the immuno-fluorescence assay. This assay, similar to the agglutination assay, relies on the use of functionalized particle to capture a target analyte. The binding created between analyte and particle is not used to create

inter-particle interactions in this case, as in the agglutination assay, but instead promotes the binding of several analytes to a single particle. Once the analyte and particles have had sufficient time to interact, a secondary antibody with a fluorescent marker is added to the solution and bonds to the analytes. Detection is accomplished by measuring the fluorescent intensity of each of the beads through a flow cytometry unit. In order to increase the sensitivity of the assay to a usable level, it must be conducted with a small number of beads with a high concentration of antibodies coating the particle. Aggregation is needed to successfully complete this assay in order to concentrate the few beads and deliver them to the detection site.[18]

Two different components are essential to aggregation assays and have been the focus of extensive engineering advancements. The first of these components is the particle used as the capture base in the aggregation assays. Many modern assays focus on the use of smaller particles as they have a higher surface area to volume ratio, increasing the amount of capture surface available to complete the assay. Nanoparticles in particular have been the focus of extensive research from a materials perspective and are essential for certain assays such as those that use changes in LSPR for detection.[17,19,20] Another reason nanoparticles are widely used in bio sensing applications is that they can be purchased at a very low cost.

The second key component that has been extensively studied that plays an important role in aggregation assays is aggregation methods. Agglutination assays can be done without any external forces, but their sensitivity, speed and limit-of-detection can be greatly enhanced by increasing the localized concentration of particles. Immune-fluorescence assays are inherently dependent on aggregation methods to function. A number of different techniques for aggregation have been studied and what follows will be a review of the more prominent approaches to controlling micro-/nanoparticles.

Aggregation Methods

Magnetophoresis

Magnetophoresis is a process that uses magnetic fields to control the motion of magnetic particles in a viscous medium. The process uses the magnetic force exerted by a magnetic gradient on these particles to overcome the viscous drag force and gravitational forces also experienced by particles. The magnetic force is proportional to the volume of the particle, as is the gravitational force on the particle. The drag force however, scales with the radius of the particle. There exists therefore a critical radius at which this process is no longer able to function as the magnetic force cannot overcome the drag force.[21] This process has been used for particle separation devices.[22] Magnetic particles can therefore be used as tags to label and isolate biological targets, and can be conducted in stationary systems as well as continuous flow systems.[23] This process exhibits a size limit in regards to the particles that can be controlled that can be improved through the use of stronger magnetic field gradients or materials with higher magnetic inductance. This process is also limited in its ability to only control magnetic particles, offering no control for polystyrene or silica particles which are common in bio-sensing applications.

Electrophoresis

Electrophoresis is similar to magnetophoresis but instead utilizes an electric field to control the movement of electrically charged particles. The electric force on a particle is independent of the size of the particle and is proportional to the electric field times the charge of

the particle. When this force is balanced with the Stokes drag force, the particle will have a velocity:

$$v = \frac{QE}{\xi} \quad (1)$$

Where ξ is the Stokes drag which is proportional to the radius of the particle. Electrophoresis does not have a size requirement for its use, but it does have practical limits as large charges and small sizes create larger velocities.[24] The most common use of electrophoresis is in gel electrophoresis, where molecules are forced through a gel by an applied electric field. The molecules often have similar charges, and therefore the distance traveled by each of the molecules is dependent on size. Within microfluidic environments, electrophoretic separation can be used on small charged particles to create label-free assays.[25] Electrophoretic forces could theoretically be used to force aggregation of particles, but they are almost exclusively used as a method for separating out particles.

Optical Control

The first successful experiment using light to control particles was conducted by A. Ashkin at Bell Labs in 1970. In his seminal paper, he describes the first use of light to create a radiation pressure, independent of heating the sample, to control the movement of microparticles.[26] In modern applications, this technology is often referred to as optical tweezers or an optical trap. The technique uses an optical gradient created by either counter-propagating laser beams, or more commonly today, a single beam focused to a diffraction-limited spot. The mechanism by which this process works is dependent on the size of the particle and the wavelength of light. There are two main ways of explaining the forces involved in optical tweezers. In the case of

micrometer sized particles, the trapping phenomena is explained by a change in momentum of light as it passes through the particle and assumes that the size of the particle is much greater than the wavelength of the light. This is known as the Mie regime. When a photon is refracted or reflected by the particle, a change in momentum in the photon occurs. According to Newton's third law, the particle must then experience an equal and opposite force. Figure 3 displays the momentum changes in the photons as well as the resulting gradient force on the particle.

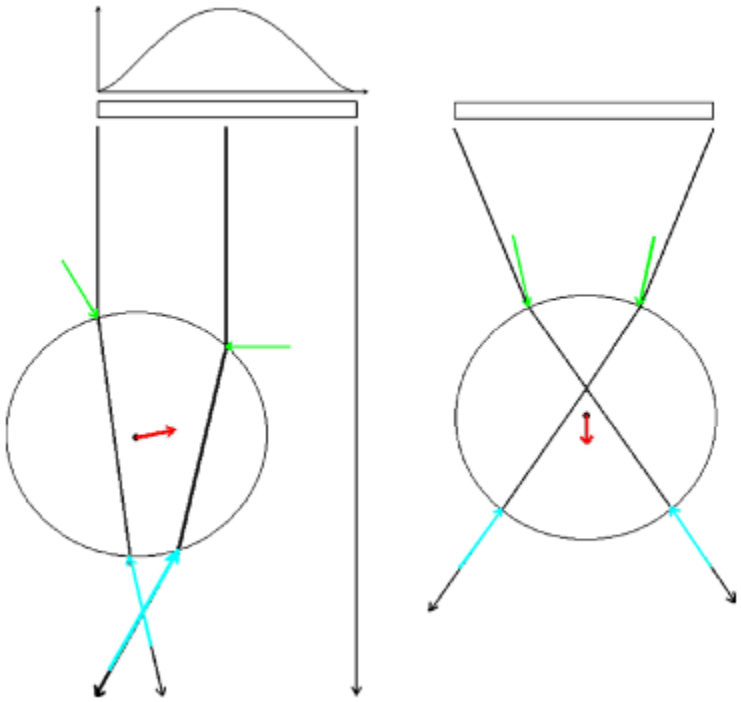

Figure 3: Radial gradient force (Left) and axial gradient force (Right) from optical beam. Green and Blue arrows represent forces from reflecting and refracting rays respectively. Red arrows represent resulting gradient forces[27]

The result of the forces exhibited by the light gradient create an initial radial focusing along the axis of the beam, followed by an outward force along the axis of the beam in the direction of the beam. The other explanation of optical trapping operates in the Rayleigh regime where it is assumed that the wavelength of the light beam is much greater than the size of the particle. In this regime, the force is explained as an electrodynamic force in which the particle, a

dipole, in a gradient electric field experiences a force in the direction of the electric field gradient. The regime in between these two is not well understood and is a current field of research.[27] This technology can be applied to a large range of size scales from atoms[28] to viruses[29] to microscale particles such as cells.[30] The forces involved in optical tweezers are often on the scale of piconewtons and therefore too weak to focus larger objects. Optical tweezers have been utilized in many applications including the sorting and separation of cells and particles as well as to aggregate those particles.[30] This technique has many advantages including the dependence on only the particles size, as well as the ability to focus a large range of particles with varying magnitude of forces. One disadvantage of this technology involves its usability outside of the lab as it normally requires expensive equipment that is not portable and requires a trained professional to operate. Biocompatibility can also be a concern when high power lasers are used to increase the force created by the optical device.

Acoustic Control

Acoustic control of particles is often done through the creation of standing pressure waves known as resonance modes. These modes are created by an acoustic wave at low frequencies combining with the speed of sound in water to create wavelengths of about 1 mm. These standing waves are reproducible, stable and controllable. They control the motion of the particle either directly, through an acoustic radiation force, or through the flow of the surrounding medium, known as acoustic streaming. The acoustic radiation force is a result of the scattering of the acoustic waves on the particle. The force from acoustic streaming experienced by a particle is a result of the viscous drag force exerted by its surrounding medium as a specific

flow pattern is induced by the acoustic wave. These forces can be supplied by either bulk acoustic waves (BAW), which travel through the body of a material, or surface acoustic waves (SAW), which travel along the surface. SAW are often preferred because they are more versatile and flexible in application as compared to BAW. SAW devices are also more energy efficient and easier to mass produce. When a SAW comes in contact with a liquid, it creates a longitudinal wave that is responsible for the acoustic radiation force and force induced by acoustic streaming. The SAW are generated by a set of Interdigital transducers (IDTs) on top of a piezoelectric substrate. A radiofrequency electric signal is directed through the IDTs, propagating mechanical stress through the piezoelectric substrate as a SAW with displacement amplitude of about 10 Å. Acoustic devices are advantageous to optical devices in that they are often simple and compact while retaining the biocompatibility of low power optical tweezers. The power and frequency used in SAW based technologies is in fact very similar to that used in ultrasonic imaging, which has been proven to be incredibly safe. One limitation however, is that existing acoustic technologies are unable to control particles smaller than ≈2 μm diameter. The purpose of this project was to explore a new acoustic resonance mode that would combine the effects of the acoustic radiation force and the force induced by acoustic streaming to allow the control of smaller particles than previously demonstrated and apply this technique to create an assay that draws on the advantages of SAW technologies.

Operating Principle

As mentioned in the Introduction, particles in an acoustic field within a fluid experience both an acoustic radiation force and a hydrodynamic viscous force (Stokes drag force) as a result of acoustic streaming. The acoustic radiation force is proportional to the radius of the particle raised to the third power. The drag force is proportional to the radius of the particle. Therefore, the radiation force is dominant in larger particle regimes, while, after a certain crossover diameter, the drag force outweighs the radiation force for smaller particles. This crossover diameter was numerically calculated by Muller et. Al. to be about 2 μm.[31] In practice, this causes many existing acoustofluidic technologies to have a lower limit on the size of particles that can be manipulated as they rely on the acoustic radiation force. If a smaller particle were placed in one of these devices, either the acoustic streaming would dominate the motion of the particle, or, in the absence of flow, by the random Brownian motion of the particle and surrounding fluid. In the case of an aggregation assay, this means that only those particles above a given diameter can be effectively focused.

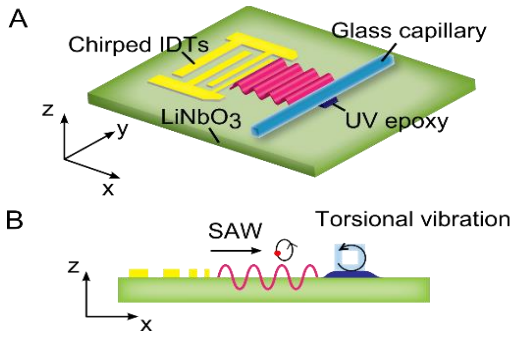

Figure 4: Schematic of device used to enrich nanoparticles

The aggregation assay presented here combines the acoustic radiation force with the acoustic streaming force to create a focusing effect in both the x- and z-direction that can operate on significantly smaller particles than the acoustic radiation force alone. The device used in the

assay, seen in Figure 4, is composed of chirped interdigital transducers (IDTs) fabricated on top of a lithium niobate ($LiNbO_3$) substrate that functions as a base for the device. The IDTs generate a surface acoustic wave (SAW) when a radio frequency is applied that travels in the x-direction towards a square glass capillary bonded to the base through a UV epoxy. The SAW travels through the substrate to the UV epoxy before propagating through the epoxy to the glass, actuating a specific vibrational mode in the square glass capillary. This action in turn creates an acoustic streaming mode with a single vortex centered on the y-axis of the capillary.

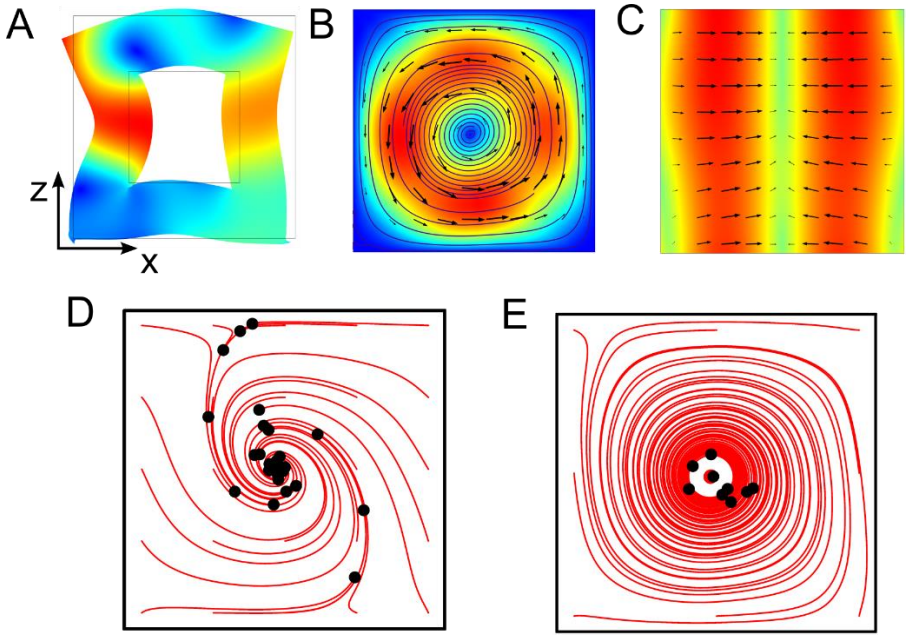

Figure 5: Results of numerical studies: A) Displacement of glass capillary walls as a result of SAW B) Streamline and velocity vectors of acoustic streaming C) Acoustic radiation force distribution D,E) Pathline and trajectories of 500 nm and 220 nm polystyrene particles respectively at 3.574 MHz

This vortex is created by the vibration of the capillary walls as shown through numerical studies. The two side walls (parallel to the y-z plane) vibrate in phase while the top and bottom walls (parallel to x-y plane) vibrate out of phase. This vibrational mode can be seen in Figure 5A at a frequency of 3.574 MHz. An animation of this mode can be found in the supplemental information of Mao et. al. 2017.[32] This torsional vibration mode creates acoustic streaming as

seen in Fig. 5B. Coupled with the acoustic radiation force as seen in Figure 5C, the two forces work together to enrich the nanoparticles in solution as seen in Figure 5D,E. It is worth noting that that similar vibrational modes were possible in non-square, non-glass capillaries as seen in the supplemental information of Mao et.al.[32]

If a particle were placed within the capillary while the SAW was being actuated, it would be forced towards the y-axis or center from a cross-sectional view. The particle would experience the acoustic radiation force shown in Fig. 5C as well as the hydrodynamic viscous force shown in Fig. 5B. For small particles (<2 μm), the acoustic radiation force would play a more minimal effect. Conversely, the acoustic streaming force would have a large impact on the motion of the particle, which would flow with the vortex created by the torsional vibration of the capillary. According to Barnkob et al.,[33] the critical diameter at which the two forces are equal can be calculated using the equation:

$$a = \sqrt{\frac{6v}{\Phi\omega}} \tag{2}$$

Where a is the critical diameter, v is the dynamic viscosity of the liquid, Φ is the acoustic contrast factor (depends on the properties of the liquid and particle), and ω is the angular velocity of the particle. For a polystyrene in a standard acoustic resonator, the critical size is around 1.6 μm. By combining the impact of both forces, even particles that are too small to be impacted by the acoustic radiation force alone can be concentrated at the center of the capillary as is shown in Figure 5E which displays the numerical focusing of 220 nm polystyrene beads. The increased path length in the 220 nm particles simulation as compared to the 500 nm simulation is due to the significantly reduced impact of the acoustic radiation force, therefore causing the smaller particles to flow in a circular vortex taking longer to focus along the center of the capillary.

Methods and Materials

The devices used to focus the particles in this study used a lithium niobate substrate (Y +128° X-propagation, Red Optronics, USA) as a base. Fabricated onto the substrate were chirped interdigital transducers (IDTs) containing twenty pairs of electrodes. The IDTs are composed of two metallic layers (Cr/Au, 50 Å/500 Å) that were added to the substrate by a photolithography process followed by an e-beam evaporation process. Two different devices were used during the experiments, the first with an operating range of 3.3-7.0 MHz and the second with an operating range of 6.3-19.8 MHz. The chirped IDTs had the electrodes spaced at linearly increasing intervals from 140 to 330 μm and from 50 to 160 μm for the first and second device respectively. The front opening for both of the chirped IDTs is 30 μm. A square cross-section glass capillary was bonded to the base using a UV epoxy (NOA 61, Norland Optical Adhesives, USA) as an adhesive. The capillary for the first device had outer dimensions of 400 μm x 400 μm x 10 mm and inner dimensions of 200 μm x 200 μm. The capillary for the second device had outer dimensions of 200 μm x 200 μm x 10 mm and inner dimensions of 100 μm x 100 μm. The capillary was placed in parallel with the IDTs at a distance of 120 μm above the substrate. UV epoxy was placed between the capillary and the substrate. The epoxy was solidified through exposure to UV light for 15 minutes.

Figure 6: UV light used to harden epoxy

The polystyrene beads (110 nm, 220 nm and 530 nm fluorescent, 500 nm non-fluorescent) were purchased from BangLabs, Inc. (USA). The silica beads (80 nm and 200 nm) were purchased from nanoComposix (USA). The bovine serum (BSA)-biotin used to coat the nanoparticles for the immunoassay was purchased from BioVision (USA). The Alexa 488-streptavidin used in the two-part assay was purchased from Invitrogen (USA). The streptavidin and DyLight 488-antistreptavidin antibody used in the three-part assay were purchased from Vector Laboratories (USA). The silica nanoparticles used in both of the immunoassays were prepared by mixing 50 µL at 10 mg/mL of nanoparticle solution with 200 µL at 2 mg/mL of BSA-biotin and incubating for 12 hours at 4 °C. The mixed nanoparticle solution was then centrifuged as 4500 g for 15 min followed by washing with phosphate buffer solution (PBS) purchased from Sigma-Aldrich (USA) to form 50 µL of washed solution. For the two-part assay, 2 µL of the washed nanoparticle solution was mixed with 20 µL of Alexa 488-streptavidin solution at concentrations of .9 nM, 1.8 nM, 9.0 nM and 18.0 nM at room temperature for 30 min to facilitate bonding between the two solutions. This was the final solution injected into the device for testing. For the three-part assay, 2 µL of the washed nanoparticle solution were mixed with 20 µL of the streptavidin solution at .9 nM, 1.8 nM, 9.0 nM, 18.0 nM and 36.0 nM

concentration for 30 min at room temperature. The two solutions were then centrifuged at 4500 g for 15 min and then mixed with 20 µL of DyLight antistreptavidin antibody solution at concentrations of 2.5 µg/mL, 5.0 µg/mL, 10.0 µg/mL and 20.0 µg/mL) at room temperature for 30 min.

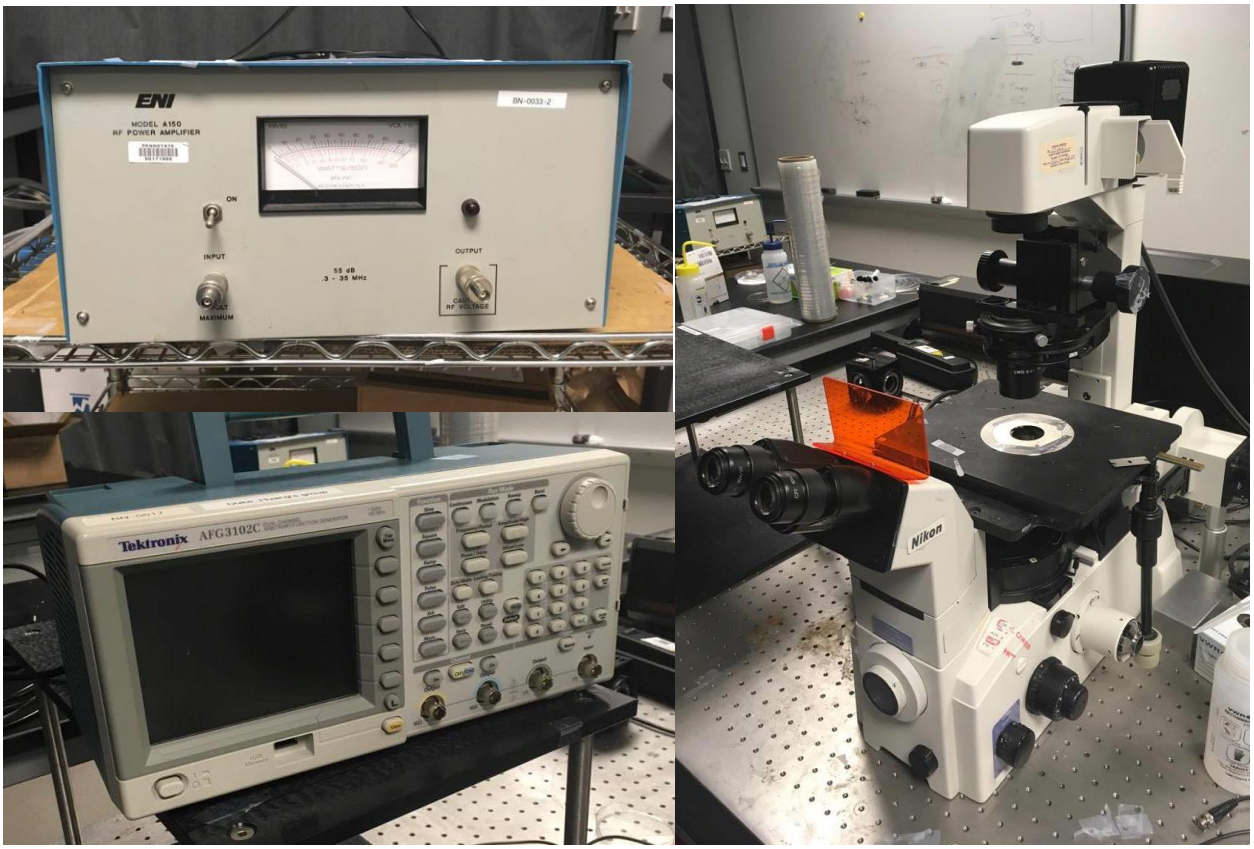

Figure 7: Equipment used to activate device and collect measurements a) power amplifier b) radio frequency function generator c) microscope

All experiments were conducted with the device attached to the stage of a microscope (TE200U, Nikon, Japan). The AC signals used to generate the SAW was created by an RF signal generator (E4422B, Agilent, USA) that was amplified (100A250A, Amplifier Research, USA) to provide the required power to activate the focusing device.

Results and Discussion

Note: the data and results discussed below where the result of a collaborative effort that resulted in the publication of Mao et al. 2017.[32]

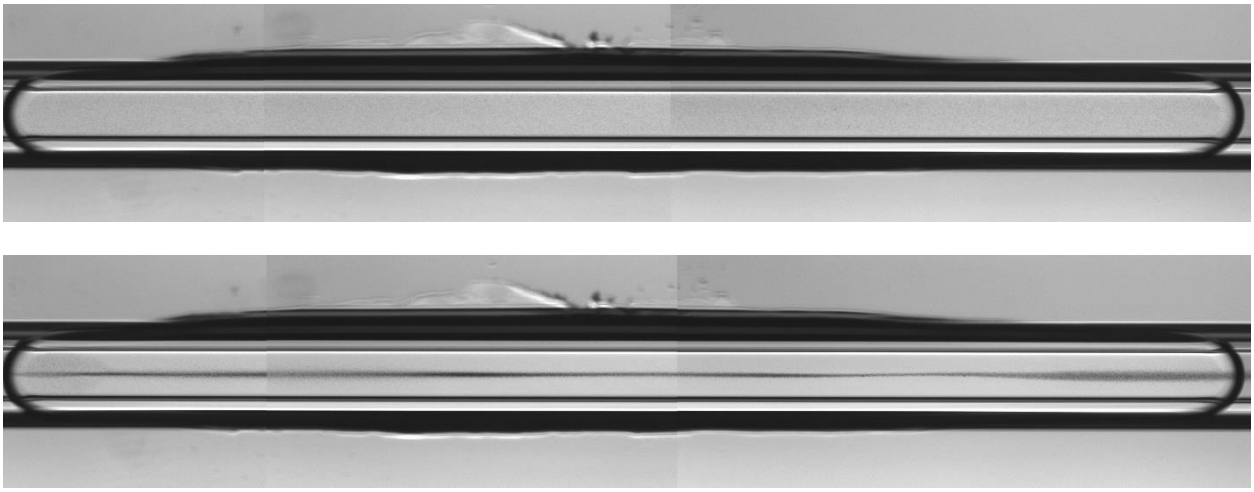

Figure 8:Image of capillary region directly above the UV epoxy before (Top) and after focusing (Bottom)

The first series of experiments conducted were intended to verify the numerical simulations of the single-vortex nanoparticle focusing process. The initial study was conducted by injecting a solution of 500 nm polystyrene particles in a PBS solution into the glass capillary. A radio frequency of 3.574 MHz was applied to the IDTs, directing SAW towards the 200 μm x 200 μm cross section glass capillary for one minute. After the activated period, images were collected in the region directly above the UV epoxy binding the capillary to the substrate. Figure 8 displays the visually identifiable focusing of particles in the center region of the capillary.

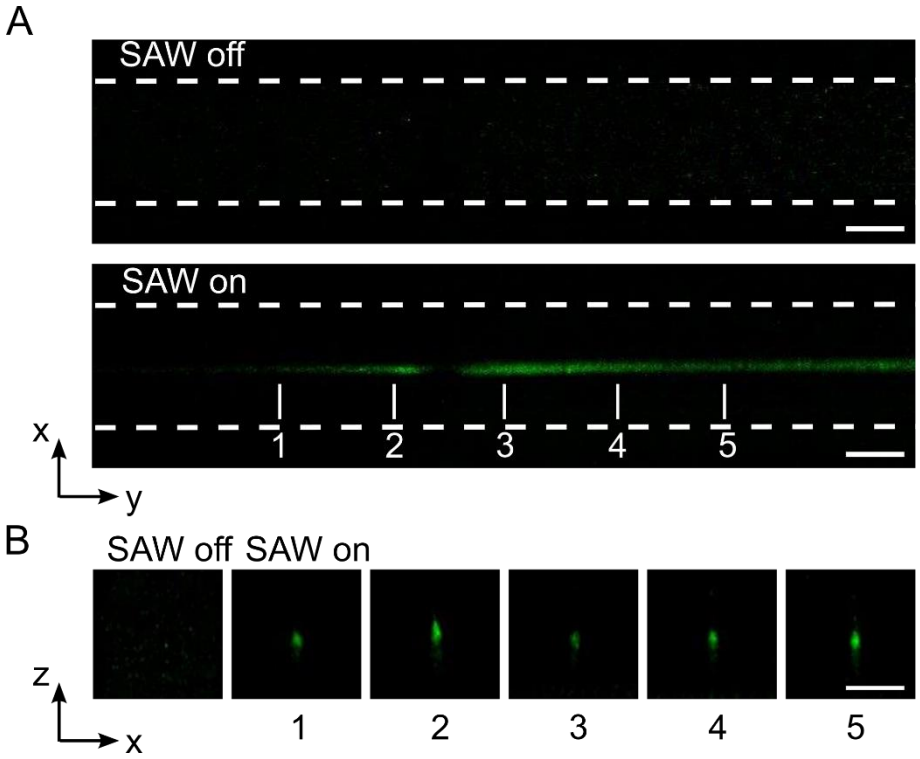

Figure 9: A) top view of glass capillary containing 530 nm fluorescent polystyrene particles before and after focusing B) cross section of glass capilary before and after focsuing displaying focusing in both the x- and z-direction. 1-5 correspond to the labeled locations in A. The scale bars represent 100 µm

Confocal microscopy was used to confirm the 2-D focusing as predicted in the numerical models. These models were replicated using fluorescent polystyrene 530 nm particles. The effective focusing region was about 2 mm away from the epoxy.

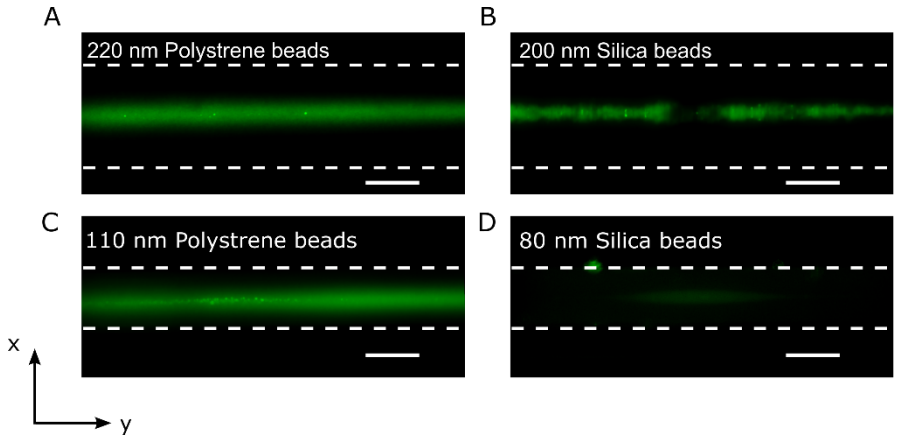

Figure 10: Experimental results of focusing 220 nm polystyrene (A) and 200 nm silica (B) beads within a 200 µm x 200 µm capillary by the activation of 3.574 MHz SAW. Focusing of 110 nm polystyrene (C) and 80 nm silica (D) beads within a 100 µm x 100 µm inner cross section glass capillary by the activation of 7.138 MHz SAW.

Following the replication of the single vortex acoustic flow that was first demonstrated numerically, further experiments were done to explore the limits of this enrichment technology. The 220 nm polystyrene particles that were initially numerically modeled were able to be completely focused at the center of the glass capillary through a spiral motion created by the hydrodynamic viscous force followed by pushing to the center by the acoustic radiation force. The 110 nm polystyrene particles were not focused as precisely. It is theorized that this is because the acoustic radiation force is much smaller for these particles, and therefore only the hydrodynamic viscous force plays a role in the concentrating of the particles. Therefore the 110 nm particles are pushed towards the general center of the capillary by the spiral flow but do not form a compact line because of the lack of an acoustic radiation force. To be able to accurately focus the 110 nm particles, manipulations were made to the device design to increase the ratio of the acoustic radiation force and the hydrodynamic viscous force. This was accomplished by increasing the frequency of the generated SAW that actuate the capillary. This was accomplished by modifying the device to operate at 7.138 MHz and the capillary to have 100 μm x 100 μm dimensions. This device was fabricated in the same way as the other device, but with a change in electrode pattern and a different capillary. Another important parameter in the ratio of forces interacting with particles in this system is the density of the individual particles. The increased density and hardness of silica particles increases the acoustic contrast force between the particles and the liquid, increasing the critical diameter and the ratio of forces. The acoustic streaming force does not account for the material of the nanoparticle, and since the acoustic radiation force increases with increases in the acoustic contrast force, the ratio of the two forces creates a more favorable environment for the focusing for smaller particles. Using these modifications to the original experiment, 110 μm polystyrene particles and 80 μm silica nanoparticles were

successfully and precisely focused. Using two different capillaries to generate the single vortex flow also suggests the ability to use the technique in a variety of capillaries with modifications needed to match the SAW to the corresponding necessary frequency in the new capillary.

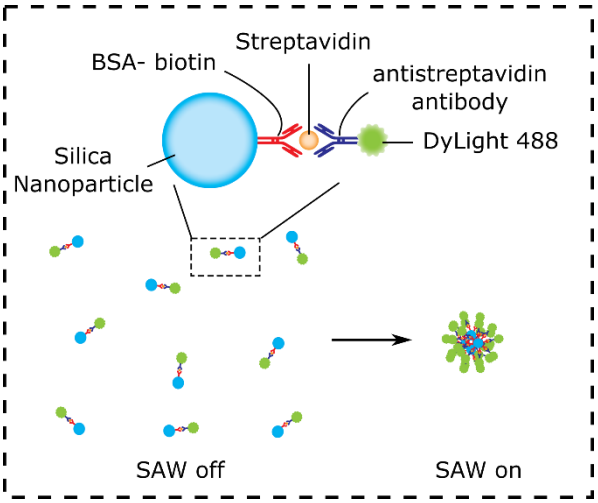

Figure 11: Initial design for homogeneous immunoassay using aggregation to control detection

In order to utilize the acoustofluidic advance of being able to focus nanoparticles within a glass capillary, we designed a homogeneous immunoassay with the hopes of coupling the aggregation force of the acoustic mechanism with the detection sensitivity of ELISA, while limiting the need for highly trained personnel. The assay consists of three main components: 1) the biomarker being detected 2) nanoparticles functionalized to antibodies for the select target, and 3) a fluorescent marker, also functionalized to attach to the select target. These three components will be referred to as the connector, anchor and marker respectively. If all three components are present, they form a conjugate that is then focused to the center of the capillary using the nanoparticle as an anchor. The relative intensity of fluorescence in the center of the channel will then increase significantly as the concentration of fluorescence markers increases. If the target biomarker, or connector, is not present however, the fluorescent marker and the nanoparticle anchor are not joined together. The fluorescent marker is too small to be focused by

either the acoustic radiation or the acoustic streaming force, and therefore the intensity of the signal at the center of the channel does not change. Instead, a diffuse, weak signal pervades throughout the capillary.

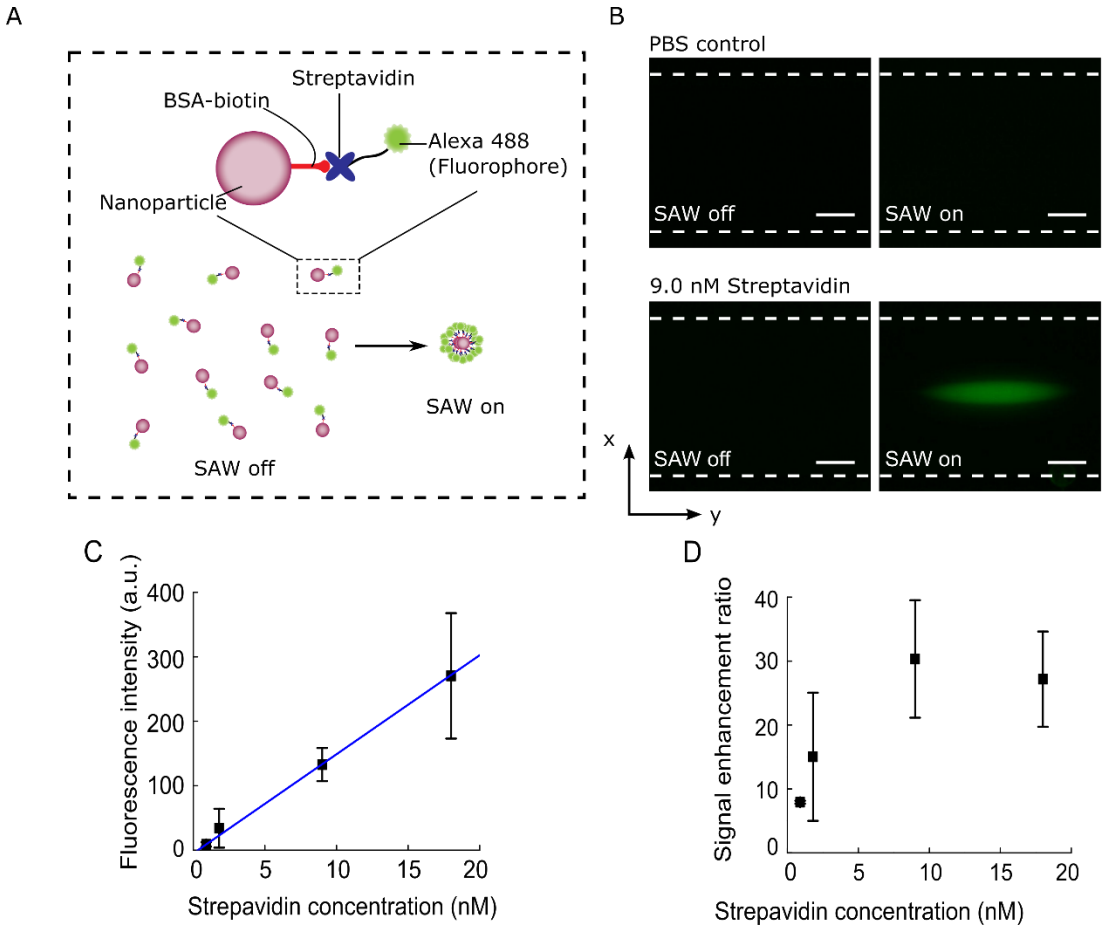

Figure 12: A) Simplified two-part assay B) Top view of glass capillary before and after activation of SAW for PBS control group (200 nm silica particle in PBS solution) and test group (200 nm silica particle and 9.0 nM streptavidin) C) Fluorescent intensity at varying streptavidin concentrations D) signal enhancement ratio at varying streptavidin concentrations

To test the viability of such an assay, we began by testing a simplified, two-part assay. Here, we used biotin-modified nanoparticles to detect streptavidin. 200 nm silica particles were prepared by coating them with bovine serum biotin. In preparation for the immunoassay, the nanoparticles were mixed with Alexa 488 labeled streptavidin in a PBS solution for 30 min. After mixing, the solution was injected into the capillary where images were collected before and

after activating the SAW to measure the change in fluorescent intensity. Figure 12B compares fluorescent images taken before and after activating the SAW to establish the torsional vibrational mode in the glass capillary, as well as a control experiment in which no fluorescent markers were added. In the control, the biotin-coated nanoparticles are injected into the capillary in a PBS solution without the addition of the fluorescently labeled streptavidin. In the main experiment, a clear change in relative fluorescent intensity is visible to the naked eye. The silica particle serves as an anchor when attached to the streptavidin molecule, effectively dragging it along as the silica nanoparticles are focused due to the single vortex flow within the capillary. In the "off" condition for the experiment, a very weak background fluorescent signal can be measured by a high-sensitivity CMOS camera due to the randomly dispersed fluorescent markers. However, the "on" case displayed a significant enhancement factor and therefore requires no further washing or purification steps for analysis.

Once the viability of the assay was confirmed qualitatively, the next test was to explore the use of this assay in a quantitative mode. Experiments were conducted by maintaining the nanoparticle- biotin concentration constant while varying the concentration of the prepared streptavidin from .09 nM to 18 nM. Fluorescent intensity measurements were collected after activation of the single vortex flow and compared to pre-focusing images. This data is plotted in Fig. 12C and displays a very strong linear correlation between streptavidin concentration and fluorescent intensity. This linear relationship enables the quantification of unknown samples as the concentration can easily be calculated from the fluorescence intensity measurement. Furthermore, the fluorescent intensity measurements after focusing were compared to those collected before focusing. The samples displayed a ≈10-30-fold enhancement for the .09 nM and 18 nM samples respectively.

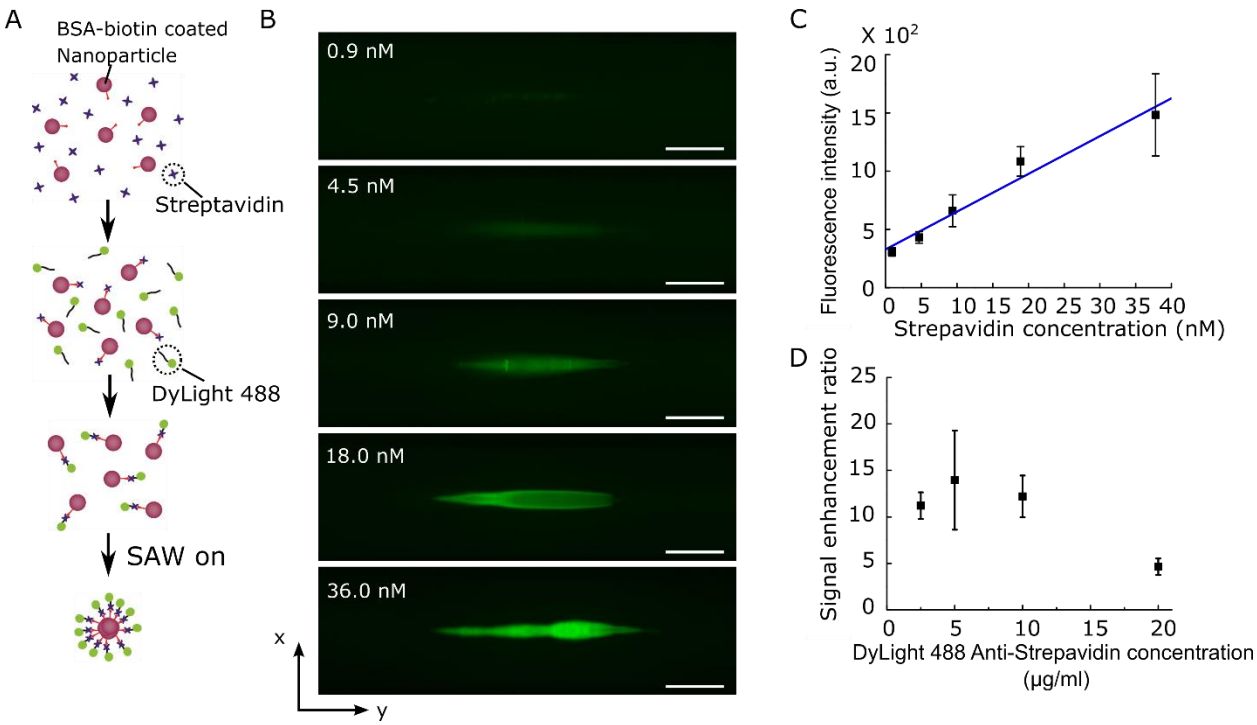

Figure 13: A) schematic of full three-part assay B) Fluorescent images collected using varying concentrations of streptavidin within an environment with 200 nm silica particles and fixed antibody concentration C) Fluorescent intensity with respect to varying streptavidin concentration D) Signal enhancement ratio with respect to varying fluorescent markers

While useful in displaying the possible advantages to bioassays, this set of experiments relied on an oversimplified model to confirm its viability. As an acoustofluidic immunoassay, this technology must be able to detect streptavidin concentration without any prior labeling. In the previous studies, the fluorescent markers were attached to the streptavidin before mixing with the nanoparticles. To further explore the viability of an acoustofluidic immunoassay based on the enrichment of nanoparticles within a capillary more studies were required where the target molecule did not have any modifications before the monitoring step. In the new assay, three different components were mixed together prior to injection in the capillary. These three parts correspond to the components of the earlier described planned assay. Biotin coated silica nanoparticles were once again used in this assay. The target in the assay is streptavidin molecules

with varying concentrations. The marker for this assay was a DyLight 488 fluorescent dye attached to an anti-streptavidin antibody. In order to promote the binding of each of the components of the assay, the streptavidin molecules were mixed with the biotin-coated nanoparticles for 30 minutes, followed by mixing of the solution with the fluorescent markers. Following the one hour preparation period, the solution was injected into the capillary just as in the previous assay. Once the solution is loaded in the capillary, the SAW were activated, focusing the nanoparticles and attached molecules to the center of the channel. Figure 13B displays the fluorescent enhancement that occurs after the activation of the acoustic focusing. A control sample of nanoparticles and fluorescent markers was prepared without the streptavidin to serve as a connector. In this control configuration, no signal change is detected because the fluorescent dye and antibody are too small to be affected by either the acoustic radiation force or the acoustic streaming force. Brownian motion dominates in this regime and therefore the molecules remain randomly dispersed in the capillary after applying the SAW. It is expected that the nanoparticles were focused in the control experiment based on the earlier results, although they cannot be detected through fluorescent imaging. This differentiation in focusing capabilities between the streptavidin solution and PBS control solution is the foundation for the acoustofluidic immunoassay.

Similar to the simplified assay, further experiments were needed to confirm the viability of the three-part assay as a quantitative tool as well as a qualitative one. The first test maintained a constant concentration of nanoparticles and fluorescent markers (2.5 μg/ml) with the concentration of streptavidin as the independent variable. Streptavidin concentrations were varied from .9 nM to 36 nM. As in the two-part assay, a linear relationship was observed between the concentration of the target molecule and the fluorescent intensity detected. These

results confirm the quantitative capabilities of the more general and realistic three-part assay that functions as a homogenous immunoassay. Figure 13B also investigated the role of changing the marker concentration from 2.5 μg/ml to 20.0 μg/ml while maintaining the streptavidin concentration constant at 18.0 nM. Marker concentration displayed an inverse parabolic relationship with signal enhancement ratio. Increasing anti-streptavidin concentration at first increases the signal enhancement ration before reaching a peak at around 5.0 μg/ml. Further increases in DyLight 488 anti-streptavidin concentration resulted in a decrease in signal enhancement. It is theorized that this occur because the maximum amount of possible bonding occurs at 5 μg/ml while any further increase does not result in the formation of any further three-part conjugates because all the streptavidin molecules are already being used. Therefore, increasing the concentration of the fluorescent markers increases the background signal before activating the SAW but does not result in any change in the concentrated signal after focusing.

Conclusion

The detection process using this platform is exceedingly simple in relation to existing tests such as ELISA because it requires a single step for detection. Once the sample is injected, the SAW must be turned on for a set period of time and then detection can take place immediately afterwards. No intermediate washing step is required because the relative change in fluorescent intensity is sufficient to differentiate between a range of concentrations along a linear scale. The preparation for this procedure consists of mixing all the components of the assay together, a task that could be completed in a microfluidic environment. Integration of this assay with other microfluidic components open the door to utilization by non-highly trained personnel

(as ELISA requires). Coupled with high speeds, low power requirements and quantitative capabilities, this assay has exciting potential for point-of-care applications as diagnostic and monitoring tool that can take treatment out of the lab and to the bedside or home of patients.

BIBLIOGRAPHY

(1) Canadian Medical Protective Association, T. *The Diagnosis: It Starts with Assessment*; 2015.

(2) Richardson, W. S.; Wilson, M. Users' Guides to the Medical Literature: A Manual for Evidence-Based Clinical Practice. In; Gordon Guyatt, Ed.; McGraw-Hill: New York, NY, 2014; p. 736.

(3) Manuals Staff. Common Medical Tests. *Merck Manual*.

(4) Cristofanilli, M.; Budd, G. T.; Ellis, M. J.; Stopeck, A.; Matera, J.; Miller, M. C.; Reuben, J. M.; Doyle, G. V.; Allard, W. J.; Terstappen, L. W. M. M.; *et al.* Circulating Tumor Cells, Disease Progression, and Survival in Metastatic Breast Cancer. *N. Engl. J. Med.* **2004**, *351*, 781–791.

(5) Vaidya, V. S.; Ramirez, V.; Ichimura, T.; Bobadilla, N. A.; Bonventre, J. V. Urinary Kidney Injury Molecule-1: A Sensitive Quantitative Biomarker for Early Detection of Kidney Tubular Injury. *Am. J. Physiol. - Ren. Physiol.* **2006**, *290*.

(6) Vigil, A.; Condés, E.; Vigil, L.; Gallar, P.; Oliet, A.; Ortega, O.; Rodriguez, I.; Ortiz, M.; Herrero, J. C.; Mon, C.; *et al.* Cystatin C as a Predictor of Mortality and Cardiovascular Events in a Population with Chronic Kidney Disease. *Int. J. Nephrol.* **2014**, *2014*.

(7) Lu, J.-J.; Tsai, F.-J.; Ho, C.-M.; Liu, Y.-C.; Chen, C.-J. Peptide Biomarker Discovery for Identification of Methicillin-Resistant and Vancomycin-Intermediate Staphylococcus Aureus Strains by MALDI-TOF. *Anal. Chem.* **2012**, *84*, 5685–5692.

(8) Gabriely, G.; Yi, M.; Narayan, R. S.; Niers, J. M.; Wurdinger, T.; Imitola, J.; Ligon, K. L.;

Kesari, S.; Esau, C.; Stephens, R. M.; *et al.* Human Glioma Growth Is Controlled by microRNA-10b. *Cancer Res.* **2011**, *71*, 3563–3572.

(9) Shao, H.; Chung, J.; Balaj, L.; Charest, A.; Bigner, D. D.; Carter, B. S.; Hochberg, F. H.; Breakefield, X. O.; Weissleder, R.; Lee, H. Protein Typing of Circulating Microvesicles Allows Real-Time Monitoring of Glioblastoma Therapy. *Nat. Med.* **2012**, *18*, 1835–1840.

(10) Skog, J.; Würdinger, T.; van Rijn, S.; Meijer, D. H.; Gainche, L.; Sena-Esteves, M.; Curry, W. T.; Carter, B. S.; Krichevsky, A. M.; Breakefield, X. O. Glioblastoma Microvesicles Transport RNA and Proteins That Promote Tumour Growth and Provide Diagnostic Biomarkers. *Nat. Cell Biol.* **2008**, *10*, 1470–1476.

(11) Freeman, E. W.; Sammel, M. D.; Lin, H.; Gracia, C. R. Anti-Mullerian Hormone as a Predictor of Time to Menopause in Late Reproductive Age Women. *J. Clin. Endocrinol. Metab.* **2012**, *97*, 1673–1680.

(12) Boster Biological Technology. ELISA kits , ELISA principle - Immunoassays https://www.bosterbio.com/protocol-and-troubleshooting/elisa-principle (accessed Feb 26, 2017).

(13) Laterza, O. F.; Price, C. P.; Scott, M. G. Cystatin C: An Improved Estimator of Glomerular Filtration Rate?

(14) Cytodiagnostics Inc. Lateral Flow Immunoassays http://www.cytodiagnostics.com/store/pc/Lateral-Flow-Immunoassays-d6.htm (accessed Feb 26, 2017).

(15) Molina-Bolívar, J. A.; Galisteo-González, F. Latex Immunoagglutination Assays. *J. Macromol. Sci. Part C Polym. Rev.* **2005**, *45*, 59–98.

(16) Singer, J. M.; Plotz, C. M.; Ragan, C.; Jacobson, S. H.; Rivera, E. U.; Marks, H. G. The

Latex Fixation Test. *Am. J. Med.* **1956**, *21*, 888–892.

(17) Mancuso, M.; Jiang, L.; Cesarman, E.; Erickson, D. Multiplexed Colorimetric Detection of Kaposi's Sarcoma Associated Herpesvirus and Bartonella DNA Using Gold and Silver Nanoparticles. *Nanoscale* **2013**, *5*, 1678–1686.

(18) Wiklund, M.; Toivonen, J.; Tirri, M.; Hänninen, P.; Hertz, H. M. Ultrasonic Enrichment of Microspheres for Ultrasensitive Biomedical Analysis in Confocal Laser-Scanning Fluorescence Detection. *J. Appl. Phys.* **2004**, *96*, 1242–1248.

(19) Li, M.; Kang, J. W.; Dasari, R. R.; Barman, I. Shedding Light on the Extinction-Enhancement Duality in Gold Nanostar-Enhanced Raman Spectroscopy. *Angew. Chemie* **2014**, *126*, 14339–14343.

(20) Esenturk, E. N.; Hight Walker, A. R. Gold Nanostar @ Iron Oxide Core–shell Nanostructures: Synthesis, Characterization, and Demonstrated Surface-Enhanced Raman Scattering Properties. *J. Nanoparticle Res.* **2012**, *15*, 1364.

(21) Yan, H.; Wu, H. Magnetophoresis. In *Encyclopedia of Microfluidics and Nanofluidics*; Springer US: Boston, MA, 2008; pp. 1043–1048.

(22) Bor Fuh, C.; Chen, S. Y. Magnetic Split-Flow Thin Fractionation: New Technique for Separation of Magnetically Susceptible Particles. *J. Chromatogr. A* **1998**, *813*, 313–324.

(23) Pamme, N.; Wilhelm, C.; Rathnayaka, K. D. D.; Rodriguez, A.; Chalmers, J. J.; Zborowski, M.; Bacri, J. C.; Michel, J. B.; Letourneur, D.; Deux, J. F.; *et al.* Continuous Sorting of Magnetic Cells via on-Chip Free-Flow Magnetophoresis. *Lab Chip* **2006**, *6*, 974.

(24) Dorfman, K. D. Electrophoresis. In *Encyclopedia of Microfluidics and Nanofluidics*; Springer New York: New York, NY, 2015; pp. 926–934.

(25) Manz, A.; Graber, N.; Widmer, H. M. Miniaturized Total Chemical Analysis Systems: A Novel Concept for Chemical Sensing. *Sensors Actuators B Chem.* **1990**, *1*, 244–248.

(26) Ashkin, A. Acceleration and Trapping of Particles by Radiation Pressure. *Phys. Rev. Lett.* **1970**, *24*, 156–159.

(27) Kumar, A.; Ewing, A. H.; Wereley, S. T. Optical Tweezers for Manipulating Cells and Particles. In *Encyclopedia of Microfluidics and Nanofluidics*; Springer US: Boston, MA, 2008; pp. 1558–1563.

(28) Hänsch, T. W.; Schawlow, A. L. Cooling of Gases by Laser Radiation. *Opt. Commun.* **1975**, *13*, 68–69.

(29) Arias-Gonzalez, J. R. Optical Tweezers to Study Viruses. In *Structure and Physics of Viruses*; Springer Netherlands, 2013; pp. 273–304.

(30) Zhang, H.; Liu, K.-K. Optical Tweezers for Single Cells. *J. R. Soc. Interface* **2008**, *5*, 671–690.

(31) Muller, P. B.; Barnkob, R.; Jensen, M. J. H.; Bruus, H. A Numerical Study of Microparticle Acoustophoresis Driven by Acoustic Radiation Forces and Streaming-Induced Drag Forces. *Lab Chip* **2012**, *12*, 4617.

(32) Mao, Z.; Li, P.; Wu, M.; Bachman, H.; Mesyngier, N.; Guo, X.; Liu, S.; Costanzo, F.; Huang, T. J. Enriching Nanoparticles via Acoustofluidics. *ACS Nano* **2017**, *11*, 603–612.

(33) Barnkob, R.; Augustsson, P.; Laurell, T.; Bruus, H. Acoustic Radiation- and Streaming-Induced Microparticle Velocities Determined by Microparticle Image Velocimetry in an Ultrasound Symmetry Plane. *Phys. Rev. E* **2012**, *86*, 56307.

NICOLAS MESYNGIER ACADEMIC VITA

EDUCATION

- **PENN STATE UNIVERSITY PARK**
  - BS Engineering Science with minors in Physics
  - Degree expected May 2017
  - Millennium Scholars Program
  - Schreyer Honors College
  - Presidential Leadership Academy
  - Thesis Title: An Acoustically Enhanced Homogeneous Immunoassay
  - Thesis Supervisor: Prof. Francesco Costanzo

RESEARCH EXPERIENCE

- **INSTITUTE FOR NANOBIOTECHNOLOGY REU STUDENT, JOHNS HOPKINS**
  Summer 2016
  Worked full time under Prof. Ishan Barman. Developed a non-sandwich, dual-functional optical sensor for detection of toxins. Controlled the separation of a fluorescent dye from a gold nanostar using an aptamer connection as an on-off signal utilizing both SERS and fluorescence signals. Reviewed literature, designed techniques, collected data, conducted data analysis, and presented results as a poster and separately in an oral presentation.

- **UNDERGRADUATE RESEARCHER, ACOUSTOFLUIDICS LAB, PENNSYLVANIA STATE UNIVERSITY**
  September 2015 – present
  Working under Prof. Tony Huang. Investigating standing surface acoustic waves in microfluidic devices to focus and control micro- and nanoparticles. Designed an acoustic aggregation assay for low concentration detection of biomarkers. Tested and analyzed data for simplified assay, reviewed pertinent literature and prepared follow-up proposals. Paper revised and resubmitted.

- **WAVE FELLOW, NANOFABRICATION GROUP, CALIFORNIA INSTITUTE OF TECHNOLOGY**
  Summer 2015
  Worked full time under Prof. Axel Scherer. Assisted fabrication of nano-structured substrate for Surface-Enhanced Raman Spectroscopy functionalized for detection of oncogenic miRNA. Peak identification and 2-D correlation analysis conducted through Matlab. Reviewed pertinent literature, assisted in data collection and orally presented results.

- **UNDERGRADUATE RESEARCHER, PENNSYLVANIA STATE UNIVERSITY**
  October 2014- May 2015
  Worked under Prof. Susan Trolier- McKinstry. Spent time in clean room facilities researching energy harvesting devices composed of piezo-electric material. Work included but not limited to sputter and sol-gel deposition of PZT onto Nickel foil followed by electrical characterization. Presented results in a poster presentation.

- **INTERDISCIPLINARY MATERIALS AND PHYSICS REU STUDENT, PENNSYLVANIA STATE UNIVERSITY**
  Summer 2014
  Worked full time under Prof. Mauricio Terrones. Synthesized single-layered, hexagonal islands of graphene using Chemical Vapor Deposition. Characterized samples with Raman spectroscopy. Computationally analyzed vibrational properties of graphene edges using density functional tight-binding method. Presented results through both an oral and poster presentation.

PUBLICATIONS

- Z. Mao, P. Li, M. Wu, H. Bachman, **N. Mesyngier**, … T.J. Huang, Enriching Nanoparticles via Acoustofluidics, ACS Nano, 11, 6b06784 (2017)
- **N. Mesyngier**, An acoustically enhanced homogeneous immunoassay, Honors thesis, in prep.
- T. J. Wilson, C. R. Pfeifer, **N. Mesyngier**, D. J. Durian, Granular discharge rate for submerged hoppers, Papers in Physics 6, 060009 (2014)

POSTERS AND PRESENTATIONS

- **N. Mesyngier**, M. Li, I. Barman
  A dual-functional optical sensor for detection of liver toxin microcystin
  2016 C.A.R.E.S. Symposium
  Baltimore MD, July 28, 2016
- **N. Mesyngier**, S. Walavalkar, A. Scherer
  Detection of miR-10b with a SERS Substrate
  2015 Caltech SFP Summer Seminar Day
  Pasadena Ca, August 20, 2015
- **N. Mesyngier**, H. G. Yeo, T. Xue, S. Roundy, S. Trolier-McKinstry
  Piezoelectric Thin Films for Energy Harvesting Applications
  2015 Undergraduate Research Exhibition
  State College Pa, April 8, 2015
- **N. Mesyngier**, S. Feng, E. Cruz-Silva, M. Terrones
  Synthesis and Vibrational Properties of Hexagonal Graphene Islands
  2014 Penn State Summer Research Symposium
  State College Pa, July 31, 2014

AWARDS AND HONORS

- Honorable Mention for the NSF Graduate Research Fellowship (2017)
- 2017 GEM Fellow
- College of Engineering Research Initiative (CERI) Grant ($5000) (Aug 2014-May 2015)
- Advanced Self-Powered Systems of Integrated Sensors and Technologies (ASSIST) Undergraduate Research Fellows Program (Oct 2014-May 2015)
- Penn State Nominee to the Goldwater Scholarship (Dec 2015)
- The President's Freshman Award
- Robert & Myrtle Vierck Scholarship
- Dept. of Engineering Science & Mechanics General Scholarship

LEADERSHIP

- Founder of Undergraduate Research Introduction to Science and Engineering (U-RISE) Engineering program
  - Program intended to help underclassmen get involved in academic research
  - Responsible for organizing programing and establishing connections for 20 students
- Co-founder and member of Millennium Scholars Cohort Council
  - Liaison between students and administration
  - Identify and implement improvements to the Millennium Scholars program
- Undergraduate Research Society
  - Member of executive board
  - Responsible for expansion of program to engineering disciplines and labs
  - Tutor 5-10 students to help them get involved in research and establish connections with faculty
- Schreyer Career Development Program
  - Tutored undergraduate students about available opportunities and work-life balance